UC Davis
UC Davis Previously Published Works

Title

Single shot echo planar imaging (ssEPI) vs single shot turbo spin echo (ssTSE) DWI of the orbit in patients with ocular melanoma.

Permalink

https://escholarship.org/uc/item/1954575x

Journal

British Journal of Radiology, 94(1118)

Authors

Gumeler, Ekim

Parlak, Safak

Yazici, Gozde

et al.

Publication Date

2021-02-01

DOI

10.1259/bjr.20200825

Peer reviewed

FULL PAPER

Single shot echo planar imaging (ssEPI) *vs* single shot turbo spin echo (ssTSE) DWI of the orbit in patients with ocular melanoma

[1]EKIM GUMELER, MD, [1]SAFAK PARLAK, MD, [2]GOZDE YAZICI, MD, [3]ERDEM KARABULUT, [4]HAYYAM KIRATLI, MD and [1]KADER K OGUZ, MD

[1]Department of Radiology, Hacettepe University, School of Medicine, Ankara, Turkey
[2]Department of Radiation Oncology, Hacettepe University, School of Medicine, Ankara, Turkey
[3]Department of Biostatistics, Hacettepe University, School of Medicine, Ankara, Turkey
[4]Department of Ophtalmology, Hacettepe University, School of Medicine, Ankara, Turkey

Address correspondence to: Ekim Gumeler
E-mail: *ekim.gumeler@hacettepe.edu.tr*

Objectives: Diffusion weighted imaging (DWI) has become important for orbital imaging. However, the echoplanar imaging (EPI) DWI has inherent obstacles due to susceptibility to magnetic field inhomogeneities. We conducted a comparative study assessing the image quality of orbits in a patient cohort with uveal melanoma (UM). We hypothesized that single shot turbo spin echo (ssTSE) DWI would have better image quality in terms of less distortion and artifacts and yield better tissue evaluation compared to ssEPI-DWI.

Methods: ssEPI-DWI and ssTSE-DWI of orbits were obtained from 50 patients with uveal melanoma who were prospectively enrolled in the study. Distortion ratio (DR), signal-to-noise ratio (SNR), contrast-to-noise ratio (CNR), diffusion signal properties, and apparent diffusion coefficient (ADC) values were collected and compared between ssEPI-DWI and ssTSE-DWI. Two reviewers evaluated and compared the geometric distortion, susceptibility and ghosting artifacts, resolution, demarcation of ocular mass, and overall quality.

Results: A higher DR was found in ssEPI-DWI compared to ssTSE-DWI ($p < 0.001$). SNR and CNR were lower for the temporal lobe cortex ($p \leq 0.004$), but higher for melanoma in ssEPI-DWI than ssTSE-DWI ($p \leq 0.037$). Geometric distortion and artifacts were more common in ssEPI-DWI ($p < 0.001$). Resolution ($p \leq 0.013$) and overall quality ($p < 0.001$) were better in ssTSE-DWI. Ocular masses were demarcated better on ssEPI-DWI ($p \leq 0.002$). Significant negative correlations between T1 and T2 signal intensities ($r = -0.369$, $p \leq 0.008$) and positive correlations between T2 and both DWI signal intensities ($r = 0.686$ and $p < 0.001$ for ssEPI-DWI, $r = 0.747$ and $p < 0.001$ for ssTSE-DWI) were revealed.

Conclusion: With less geometric distortion and susceptibility artifacts, better resolution, and overall quality, ssTSE-DWI can serve as an alternative to ssEPI-DWI for orbital DWI.

Advances in knowledge: ssTSE-DWI can be a better alternative of diffusion imaging of orbits with less susceptibility artifact and geometric distortion compared to ssEPI-DWI.

Magnetic resonance imaging (MRI) is the imaging choice for evaluating orbital masses. Conventional MRI is commonly used in determining the location, extension of these mass and invasion to adjacent structures, and diffusion weighted imaging (DWI) has an additional role in delineating the lesion and its tissue characteristics.[1–6]

DWI is an imaging technique based on the motion of water molecules, showing restriction in highly cellular tumors due to the decrease in extracellular water molecules.[7] Single-shot echo-planar imaging (ssEPI) DWI is the widely used technique in radiology practice owing to its high speed. Unfortunately, it is highly susceptible to magnetic field inhomogeneities, therefore results in geometric distortions especially at tissue-air interfaces.[8,9] Single-shot turbo spin echo (ssTSE) DWI, on the other hand, is another technique which is less sensitive to magnetic inhomogeneities, therefore susceptibility artifacts.[9] Several studies concerning head and neck showed ssTSE-DWI had better image quality compared to ssEPI-DWI.[10–12]

Orbits neighboring the paranasal sinuses are more prone to susceptibility artifacts and geometric distortion in DWI.

In addition to geometric distortion and susceptibility artifacts, globe movement contributes to the difficulty of DWI when an intraocular lesion is encountered.

So far, the studies concerning ssTSE-DWI of orbits showed that the apparent diffusion coefficients (ADC) derived from ssTSE-DWI had better performance in discrimination between orbital inflammation and lymphoma compared to ADCs from multi shot EPI-DWI..[13] Another study demonstrated that ssTSE-DWI could discriminate viable and nonviable parts of retinoblastoma.[14]

We aimed to conduct a comparative study assessing the image quality of orbits in a patient cohort with uveal melanoma to ensure homogeneity among participants. Uveal melanoma (UM) is the most common primary intraocular tumor in adults. It arises from melanocytes residing in the stroma. About 90% of uveal melanomas arise in the choroid, 7% in the ciliary body, and 3% in the iris.[15] A previous study suggested that ssEPI-DWI is useful to differentiate the UM and benign retinal detachment.[16] We hypothesized that ssTSE-DWI would have better image quality in terms of less distortion and artifacts and yield better tissue evaluation compared to ssEPI-DWI. Our secondary aim was to reveal the DWI properties of UM and its relationship with its conventional MRI signal properties.

METHODS AND MATERIALS
This prospective study was approved by the local institutional review board and all participants gave informed written consent according to the World Medical Association Declaration of Helsinki.

Participants
Patients with a recently confirmed diagnosis of UM on fundoscopic examination by an ophthalmologist between November 2017 and May 2019 were enrolled in the study. Axial T2WI was the initial sequence and each study was checked after its acquisition. Tumors with a thickness (measurement of the shortest diameter) ≥2 mm were enrolled in the study. Patients with tumor thickness less than 2 mm, history of treatment for UM were excluded. All images were obtained prior to the initiation of treatment.

Magnetic resonance imaging data acquisition
Imaging was performed on a 1,5 T scanner (Achieva, Philips, Netherlands) equipped with an 8-channel phased-array receive head coil. The imaging protocol included axial turbo spin echo T2 (TR 3000 ms, TE 100 ms, slice thickness 3 mm, matrix 220 × 197, FOV 120 × 150 mm; with SPIR fat saturation), pre- and post-contrast axial spin echo T1 (TR 550 ms, TE 15 ms; slice thickness 3 mm, matrix 220 × 213, FOV 120 × 150 mm) weighted imaging (WI). 0,2 ml kg^{-1} gadoterate meglumine (Dotarem, Guerbet) was intravenously injected as Gd-based contrast material. DWI consisted of axial ssEPI-DWI (TR 2101 ms; TE 89 ms; slice thickness 3 mm; matrix 120 × 102; FOV 180 × 228 mm, EPI factor 51, NEX 2, parallel imaging (SENSE) factor of 2, acquisition time 43 sec, phase encoding direction: anteroposterior) and axial ssTSE-DWI (TR 7343 ms, TE 77 ms; slice thickness

3 mm, matrix 100 × 109, FOV 180 × 229 mm, TSE factor 55, NEX 3, parallel imaging (SENSE) factor of 2, acquisition time 3 min 40 sec, phase encoding direction: anteroposterior) with b-values of 0 and 1000 s mm^{-2} and was obtained before IV contrast media injection. Apparent diffusion coefficient maps were generated on the workstation provided by the vendor (Intellispace Portal, Philips, v7.01.20482).

Image analysis
An experienced radiologist measured maximum globe diameters on phase encoding direction (anteroposterior) on both b-1000 DWI and T2WI. From these measurements, we calculated distortion ratio (DR), which is the ratio of the maximum displacement in the phase encoding direction of the anatomical structure to its diameter on T2WI.[17] Maximum displacement is the difference between the maximum diameter of DWI with b,1000, and T2WI.

In order to calculate signal-to-noise ratio (SNR) and contrast-to-noise ratio (CNR) from both DWI, UM and left temporal cerebral cortex was used. Initially, a neuroradiologist manually drew region of interest (ROI) on T2WI using Siemens syngo.via vb30 software. The boundary of a tumor was defined with a reference to precontrast and postcontrast T1WIs, excluding hemorrhage. The location of the ROIs for the cerebral cortex was confirmed using T1WI. These ROIs were copied to the same location on both DWI b = 1000 and ADC maps. If any misalignment was present on DWI and ADC maps, it was corrected by the observer manually. The SI measurements and ADC values were all measured from a single slice in which the largest diameter of the lesion was observed. At the same set, SI of UM on T2WI and T1WI were also collected to reveal the relationship between the tumor signal characteristics and its diffusion properties. Visual features of the mass were also noted as hyper-iso or hypointense compared to the cerebral cortex on T1WI, T2WI, and DWI.

SNR was calculated by,

$$SNR = SI_a/SD,$$

Where SI_a was the mean signal intensity within the region of interest (ROI) and SD was the standard deviation of the baseline noise.

CNR was calculated by;

$$CNR = |SI_a\text{-}SI_c|/SD,$$

Where SI_c was the mean SI of the baseline noise, and SD was the standard deviation of baseline noise.

However, as parallel imaging techniques cause inhomogeneous noise levels throughout the image[17,18] and diffusion weighted applications may have artifacts throughout the field of view,[17] we used the left temporalis muscle for baseline noise due to its homogeneity and proximity to the globe and the temporal cerebral cortex.[17] The location of ROIs for the left temporalis muscle was confirmed by its correlation with T2WI. The SI and standard deviations (SD) were noted.

Figure 1. Presentation of geometric distortion on both DWI techniques. Anterior border of the globe is indistinct (arrows) on ssEPI-DWI (a) whereas it is well-delineated on ssTSE-DWI (b). For presentation purposes, the fusion of T2WI and DWI (c, d) and ADC (e, f) of each technique is seen. The fusion image of T2WI/ssEPI-DWI (c) demonstrates posterior distortion (arrows). T2WI/ssTSE-DWI fusion image presents with no distortion (d). The fusion of T2WI/ADC map of ssEPI-DWI (e) shows anterior and posterior distortion (arrows). The fusion of T2WI/ADC map of ssTSE-DWI has no distortion.
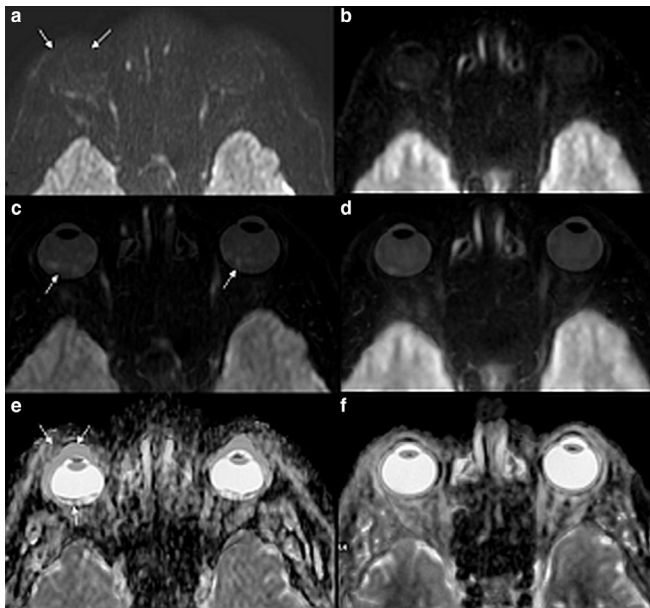
Two radiologists independently reviewed both b-1000 DWI images which were anonymized and the reviewers were blind to the sequences. Each reviewer evaluated geometric distortion; presence of susceptibility and ghosting artifacts on a five-point scale, as 1 = none, 2 = low, 3 = intermediate, 4 = high and 5 = very high, *i.e.* nondiagnostic. Resolution (defined by discrimination of orbital structures - lacrimal glands, extraocular muscles, optic nerve and lens - and intraocular mass from adjacent structures), demarcation of intraocular mass (delineation of the mass and definition of its borders), overall quality (the diagnostic competence of the image regarding all aforementioned features) were also evaluated by each reviewer, on a five-point scale: 1 = poor, 2 = below average, 3 = average, 4 = above average, 5 = excellent.

Statistical analysis

Statistical analysis was performed using the IBM SPSS Statistics software version 23. We used paired t-test to compare DR, SNR, CNR and ADC values, Wilcoxon signed ranks test to compare the nonparametric evaluation of two-DWI and Pearson correlation test to find the relationship between SI of T1, T2, and each DWI and ADC. Interobserver agreement was estimated using quadratic weighted κ (Fleiss-Cohen) for ordinal categorical variables. An overall *p*-value of less than 0.05 was considered to show a statistically significant result.

RESULTS

Fifty patients (female/male = 22/28, age-range 24–85, mean age 55.4 ± 14.5) were included in the study. ROI size changed between 5–62 mm^{-2}, with a mean 18.08 ± 10.83 mm^2 for UM and 12–24 mm^{-2}, with a mean 17.84 ± 1.73mm2 for the cerebral cortex. Summary of DR, SNR, CNR, and ADC values and their comparison are given in Table 1. DR was significantly higher on ssEPI-DWI than ssTSE-DWI ($p < 0.001$) (Figure 1). SNR and CNR were significantly higher for the temporal lobe cortex in ssTSE-DWI ($p < 0.001$ for SNR; $p \leq 0.004$ for CNR) compared to ssEPI-DWI (Table 1). However, SNR and CNR were lower on ssTSE-DWI compared to ssEPI-DWI for malignant melanoma ($p \leq 0.037$ for SNR; $p < 0.001$ for CNR) (Table 1). Mean ADC (mADC) values of both cortex and melanoma were higher on ssTSE-DWI than on ssEPI-DWI ($p < 0.001$) (Table 1). mADC of UM was significantly higher than mADC of cortex on both sequences ($p < 0.001$).

Visual imaging features of UM relative to the temporal cerebral cortex on T1 and T2WI are summarized in Table 2. The most common MRI signal was T1 hyperintensity ($n = 42$, 84% within all). Twenty four UMs demonstrated T2 hypointensity and 26 showed T2 hyperintensity. All T2 hypointense UMs were hyperintense on T1WI, constituting most of the T1 hyperintense UMs ($n = 24$, within 42 T1 hyperintense UMs). Therefore, the most

Table 1. Summary of mean DR, SNR, CNR and ADC measurements ± SDs of ssEPI-DWI and ssTSE-DWI and results of statistical comparison by paired *t*-test

	ssEPI-DWI (mean ± SD)	ssTSE-DWI (mean ± SD)	*p* value
Right DR	0.133 ± 0.085	0.047 ± 0.037	<0.001
Left DR	0.135 ± 0.102	0.037 ± 0.035	<0.001
SNR of ocular melanoma	43.87 ± 27.02	37.33 ± 18.3	0.037
SNR of temporal cortex	50.6 ± 17.17	67.08 ± 23.17	<0.001
CNR of ocular melanoma	35.56 ± 26.08	23.65 ± 16.94	<0.001
CNR of temporal cortex	42.39 ± 15.5	53.22 ± 19.36	0.004
Mean ADC of melanoma (mm^2 s^{-1})	1.108 ± 0.25 × 10^{-3}	1.298 ± 0.34 × 10^{-3}	<0.001
Mean ADC of cerebral cortex (mm^2 s^{-1})	0.86 ± 0.13 × 10^{-3}	0.915 ± 0.08 × 10^{-3}	<0.001

CNR, Contrast-to-noise ratio; DR, Distortion ratio; SNR, Signal-to-noise ratio.
Difference is significant at *p* < 0.05 level.

Table 2. Distribution of ocular melanomas (n, %) in respect of their intensity on T1- and T2WI

			T1 SI		Total
			Hyperintense	Hypointense	
T2 SI	Hyperintense	Count	18	8	26
		% within all	36%	16%	52%
	Hypointense	Count	24	0	24
		% within all	48%	0%	48%
Total		Count	42	8	50
		% within all	84%	16%	100%

common imaging feature of UM was T1 hyperintensity with T2 hypointensity (n = 24, 48% within all). These UMs most commonly showed hypointensity relative to the cerebral cortex on ssEPI-DWI (n = 17, 70.8%) and ssTSE-DWI (n = 22, 91.6%). On the other hand, all T1 hypo- and T2 hyperintense lesions (n = 8) were hyperintense on both DWI.

Pearson correlation test (Table 3) showed a significant inverse correlation between T1 and T2 (r = −0.369, $p \leq 0.008$) signal intensities of the mass. T1 SI of the mass also had a negative correlation with the SI on ssTSE-DWI (r = −0.391, $p \leq 0.005$). A weak negative correlation was present with SI of ssEPI-DWI which was not significant (r = −0.267, $p = 0.061$) (Table 3). On the other hand, T2 SI of the UM demonstrated a positive correlation with both SI of ssEPI-DWI (r = 0.686, $p < 0.001$) and ssTSE-DWI (r = 0.747, $p < 0.001$), slightly higher for ssTSE-DWI. mADC values, on the other hand, showed no correlation with T1 and T2 characteristics of the tumors.

Both reviewers independently scored high geometric distortion, susceptibility, and ghosting artifacts on ssEPI-DWI ($p < 0.001$). However, demarcation and delineation of the mass were better in ssEPI-DWI than ssTSE-DWI ($p < 0.001$ for the first reviewer, $p \leq 0.002$ for the second reviewer). Resolution ($p \leq 0.013$ for the first reviewer, $p < 0.001$ for the second reviewer) and overall quality ($p < 0.001$ for both reviewers) were better in ssTSE-DWI than ssEPI-DWI (Table 4). κ ranged between moderate to good (0.542–0.755) for each feature of both DWI techniques, shown in Table 5.

DISCUSSION

Our study aimed to find out which DWI technique had better utility for intraocular mass imaging. We demonstrated that geometric distortion was significantly lower in ssTSE-DWI. SNR and CNR were higher in ssTSE-DWI when the cerebral cortex was taken into account, however, it was the opposite when it was calculated based on UM. Independent reviewers also found higher artifacts in ssEPI-DWI. Despite demarcation of the UM was better in ssEPI-DWI, resolution and overall quality were higher in ssTSE-DWI.

As expected, we found higher DR and geometric distortion in ssEPI-DWI than in ssTSE-DWI, agreeing with the literature[10,11,19–22] (Figure 1). In the echoplanar imaging technique, multiple lines of k-space are filled after a single 90^0 focusing and 180^0 refocusing pulse, by oscillating frequency encoding gradients and blipped phase encoding gradients. Each oscillation of frequency encoding gradient represents a line in k-space and each blip of phase encoding gradient represents a transition of the lines.[8] Lack of refocusing pulses makes ssEPI-DWI sensitive to phase coherence loss, most prominent at inhomogeneous magnetic fields, such as air-tissue boundaries; and determination of the signal by T2* decay also contributes to distortion.[8] However, ssTSE uses multiple 180^0-refocusing pulses with different phase encoding gradients and fills the whole of k-space in a single excitation.[9] These refocusing pulses make it less sensitive to magnetic field inhomogeneities than ssEPI-DWI.[9]

Table 3. The relationship between signal intensities of ocular melanoma

		T2 WI	T1 WI	ssEPI - DWI	ssTSE - DWI	mADC (ssEPI)	mADC (ssTSE)
T2	Pearson's r	1	−0.369[a]	0.686[a]	0.747[a]	−0.23	0.209
	p		0.008	0.000	0.000	0.873	0.145
T1	Pearson's r	−0.369[a]	1	−0.267	−0.391[a]	−0.191	−0.09
	p	0.008		0.061	0.005	0.184	0.534

[a]means correlation is significant at *p* < 0.05.

Despite higher geometric distortion, ssEPI-DWI yielded better demarcation and delineation of the ocular masses. The edges of the masses were blurry on ssTSE-DWI as seen in Figure 2. As the signal in ssTSE-DWI is determined by the T2 transverse relaxation time, instead of T2* decay like in ssEPI-DW,[22–24] the lengthy T2 readout may have resulted in blurring.[23,24] Also, ocular movement during this long acquisition time might contribute to the blurring of the margins. Despite blurring, the overall quality was still better for ssTSE-DWI. However, the lengthy T2 readout time also causes ssTSE-DWI to have a longer acquisition time compared to ssEPI-DWI, which in turn may reduce its use on daily clinical practice.

ssTSE-DWI achieved higher SNR and CNR for the temporal cortex but lower SNR and CNR for melanoma. Similar to the temporal cerebral cortex in our study, SNR of brain parenchyma, tongue, parotid, submandibular glands, and superior deep cervical lymph nodes on 3 T scanners demonstrate higher SNR in ssTSE-DWI compared to ssEPI-DWI.[10–12,23] However, in higher magnetic fields (7T), the SNR of brain parenchyma was lower in ssTSE-DWI.[20,23] As our study used a lower magnetic field (1.5T scanner), which may contribute to higher SNR of the temporal cortex on ssTSE-DWI. Also, studies showed that SNR of ssTSE-DWI tended to be homogeneous throughout the brain,

whereas ssEPI-DWI demonstrates signal loss in the anterior and inferior parts of the brain due to magnetic field inhomogeneities.[20] The SI of the cortex was collected from the temporal lobe in our study because of its proximity to the orbits, which might contribute to the lower SNR of ssEPI-DWI. Also, various parameters, such as field of view, slice thickness, bandwidth, number of excitations (NEX) affect SNR, but apart from other parameters, NEX was slightly higher in ssTSE-DWI (3 *vs* 2 in ssEPI-DWI) in our study. The smaller NEX value of ssEPI-DWI in our study may have a small contribution to lower SNR and CNR values of ssEPI-DWI in the temporal cerebral cortex. So, in addition to NEX values, lower magnetic strength (1.5T) of the scanner and adjacent inhomogeneous magnetic field may have contributed to the differences in SNR of the temporal cerebral cortex yielded by two different DWI sequences used in this study.

In contrast to the temporal cerebral cortex, UM demonstrated lower SNR values in ssTSE-DWI compared to ssEPI-DWI. Most of the UMs were T2 hypointense and T1 hyperintense (48%) and these tumors were, mostly hypointense on ssTSE-DWI (*n* = 22), too. We also found that T2 signal intensity directly correlates with the signal intensity of DWI (Table 3), more so with ssTSE-DWI. This T2 blackout effect is more significant on ssTSE-DWI, as the signal intensity is determined by T2 decay. This might be a

Table 4. Comparison of qualitative scores of each reviewer for DWI techniques

		Median for reviewer 1	Interquartile range for reviewer 1 (25%–75%)	*p*-value for reviewer 1	Median for reviewer 2	Interquartile range for reviewer 2 (25%–75%)	*p* value for reviewer 2
Geometric distortion[a]	ssEPI-DWI	3	3–3	<0.001[c]	3	2–3	<0.001[c]
	ssTSE-DWI	1	1–1		1	1–1	
Artifacts[a]	ssEPI_DWI	2	2–3	<0.001[c]	2	2–3	<0.001[c]
	ssTSE-DWI	2	1–2		2	1–2	
Resolution[b]	ssEPI_DWI	4	3–4	0.013[d]	4	3–4	<0.001[d]
	ssTSE-DWI	4	4–5		4	4–5	
Demarcation[b]	ssEPI_DWI	4	4–5	<0.001[c]	4	3–5	0.002[c]
	ssTSE-DWI	3	3–4		3	2–4	
Overall quality[b]	ssEPI_DWI	4	4-5	<0.001[d]	3	3–4	<0.001[d]
	ssTSE-DWI	5	4–5		4	4–5	

[a]Having more negative ranks means higher quality for geometric distortion and artifacts.
[b]Having more positive ranks means higher quality for resolution, demarcation and overall quality.
[c]ssTSE-DWI had more negative ranks.
[d]ssTSE-DWI had more positive ranks.

Table 5. Interreviewer agreement for qualitative evaluation

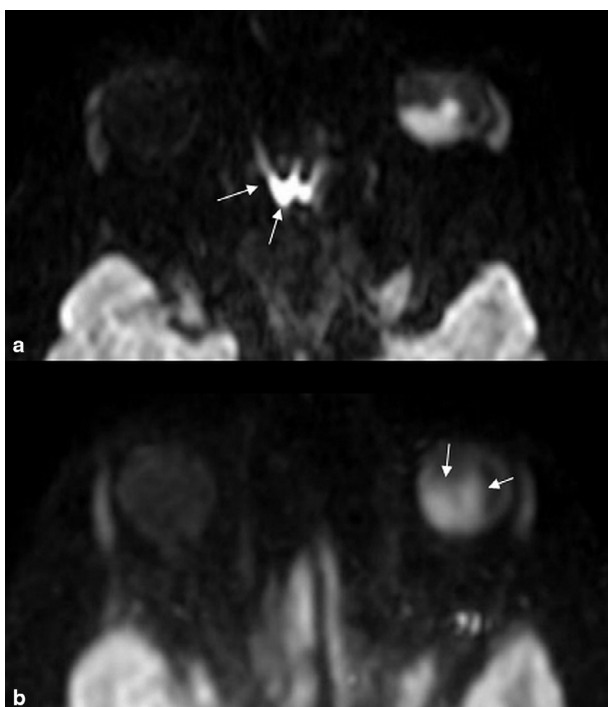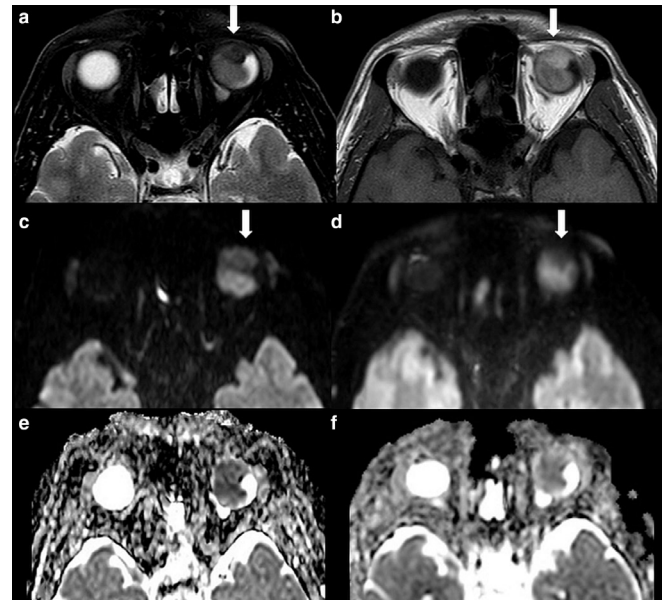|		Weighted κ
Geometric distortion	ssTSE-DWI	0.638
	ssEPI-DWI	0.626
Artifacts	ssTSE-DWI	0.644
	ssEPI-DWI	0.542
Resolution	ssTSE-DWI	0.609
	ssEPI-DWI	0.668
Demarcation	ssTSE-DWI	0.692
	ssEPI-DWI	0.697
Overall quality	ssTSE-DWI	0.717
	ssEPI-DWI	0.755

Figure 3. Bilobulated heterogeneous intraocular mass has an anterior part (arrows) which is more hypointense on T2WI (a) and more hyperintense on T1WI (b). Anterior tumor component with more profound T2 hypointensity shows relatively low signal intensity on both ssEPI-DWI (c) and ssTSE-DWI (d), more prominent on ssTSE-DWI. The lesions are visually homogeneous on ADC maps (e, f).

reason for the lower SNR of ssTSE-DWI for UM. On the other hand, ocular movement during the longer acquisition time of ssTSE-DWI might contribute to the loss of signal intensity. So the conflict in SNR values of the cerebral cortex and UM may be due to inherent tissue characteristics of UM and ocular movement effect. Further studies on different tumor types are needed to investigate this effect. On the other hand, our study involved only UMs and no benign lesions. Therefore a comparison of the diagnostic quality of these techniques in terms of discrimination between malignant and benign lesions and how SNR and CNR contribute to this discrimination could not be established. It is an important limitation of our study. Further studies including

Figure 2. Same intraocular lesion on both DWI. ssEPI-DWI (A) shows a well-demarcated lesion. Notice the susceptibility artifacts around ethmoid air cells (arrows, a). The lesion has blurry margins on ssTSE-DWI (arrows, b).

both malignant and benign intraocular and intraorbital lesions are needed to investigate diagnostic decisions.

In this study calculated mean ADC values of the cerebral cortex and ocular melanoma on ssEPI-DWI were similar to previous reports on 1.5T scanners.[25–28] However, the mADC of the cerebral cortex on ssTSE-DWI was lower (0.798×10^{-3} mm^2 s^{-1}) on previous studies performed at 7T magnetic field strength.[20]

There are controversial reports on the effect of the amount of melanin on MR imaging characteristics.[29–34] *In-vivo* imaging of melanoma at 11.7T MRI demonstrated that only the amount of melanin had no correlation with T1 and T2 SI but suggested that both melanin pigment, metal ions, and their interaction affected T1 and T2 SI of the tumor.[34] In this study, we showed that both DWI signal intensity had an inverse correlation with T1 and direct correlation with T2 signal intensities of the tumor, while ADC values had no correlation (Figure 3). Because the amount of melanin or metal ions were not detected histopathologically, their effects on T2, T1, and DWI signal intensities cannot be known. Whatever the contribution of the melanin and accompanying metal ions are, T1 and T2 signal intensity changes are related to ssTSE-DWI more.

Lack of histopathologic diagnosis can be considered as a limitation of this study. However, current medical practice applies the diagnosis of malignant melanoma based on fundoscopic examination with high accuracy.[35] This study was carried out in a single tertiary care institution, which limited the number of patients participated. Although the interobserver agreement was

good, we believe that further investigations in different institutions are needed to confirm reproducibility.

CONCLUSION

Prominent T2 effects, signal loss in the intraocular mass, and less definite demarcation of the lesion are the main shortcomings of ssTSE-DWI. Nonetheless, less geometric distortion and susceptibility artifacts, better resolution, and overall quality suggest ssTSE-DWI as a better alternative to ssEPI-DWI for orbital DWI.

PATIENT CONSENT

Informed consent was obtained from all individual participants included in the study.

ETHICS APPROVAL

All procedures performed in the studies involving human participants were in accordance with the ethical standards of the institutional and/or national research committee and with the 1964 Helsinki Declaration and its later amendments or comparable ethical standards.

REFERENCES

1. Sepahdari AR, Aakalu VK, Setabutr P, Shiehmorteza M, Naheedy JH, Mafee MF. Indeterminate orbital masses: restricted diffusion at MR imaging with echo-planar diffusion-weighted imaging predicts malignancy. *Radiology* 2010; **256**: 554–64. doi: https://doi.org/10.1148/radiol.10091956

2. Sepahdari AR, Kapur R, Aakalu VK, Villablanca JP, Mafee MF. Diffusion-weighted imaging of malignant ocular masses: initial results and directions for further study. *AJNR Am J Neuroradiol* 2012; **33**: 314–9. doi: https://doi.org/10.3174/ajnr.A2747

3. Sepahdari AR, Politi LS, Aakalu VK, Kim HJ, Razek AAKA, Abdel Razek AAK. Diffusion-weighted imaging of orbital masses: multi-institutional data support a 2-ADC threshold model to categorize lesions as benign, malignant, or indeterminate. *AJNR Am J Neuroradiol* 2014; **35**: 170–5. doi: https://doi.org/10.3174/ajnr.A3619

4. Razek AAKA, Elkhamary S, Mousa A. Differentiation between benign and malignant orbital tumors at 3-T diffusion MR-imaging. *Neuroradiology* 2011; **53**: 517–22. doi: https://doi.org/10.1007/s00234-011-0838-2

5. Xu X-Q, Hu H, Su G-Y, Liu H, Shi H-B, Wu F-Y. Diffusion weighted imaging for differentiating benign from malignant orbital tumors: diagnostic performance of the apparent diffusion coefficient based on region of interest selection method. *Korean J Radiol* 2016; **17**: 650–6. doi: https://doi.org/10.3348/kjr.2016.17.5.650

6. Sun B, Song L. Orbital malignant lesions in adults: multiparametric MR imaging. *Jpn J Radiol* 2017; **35**: 454–62. doi: https://doi.org/10.1007/s11604-017-0653-8

7. Baliyan V, Das CJ, Sharma R, Gupta AK. Diffusion weighted imaging: technique and applications. *World J Radiol* 2016; **8**: 785. doi: https://doi.org/10.4329/wjr.v8.i9.785

8. Poustchi-Amin M, Mirowitz SA, Brown JJ, McKinstry RC, Li T. Principles and applications of echo-planar imaging: a review for the general radiologist. *Radiographics* 2001; **21**: 767–79. doi: https://doi.org/10.1148/radiographics.21.3.g01ma23767

9. Dietrich O, Biffar A, Baur-Melnyk A, Reiser MF. Technical aspects of MR diffusion imaging of the body. *Eur J Radiol* 2010; **76**: 314–22. doi: https://doi.org/10.1016/j.ejrad.2010.02.018

10. Hirata K, Nakaura T, Okuaki T, Kidoh M, Oda S, Utsunomiya D, et al. Comparison of the image quality of Turbo spin echo- and echo-planar diffusion-weighted images of the oral cavity. *Medicine* 2018; **97**: e0447. doi: https://doi.org/10.1097/MD.0000000000010447

11. Mikayama R, Yabuuchi H, Sonoda S, Kobayashi K, Nagatomo K, Kimura M, et al. Comparison of intravoxel incoherent motion diffusion-weighted imaging between turbo spin-echo and echo-planar imaging of the head and neck. *Eur Radiol* 2018; **28**: 316–24. doi: https://doi.org/10.1007/s00330-017-4990-x

12. Panyarak W, Chikui T, Yamashita Y, Kamitani T, Yoshiura K. Image quality and ADC assessment in turbo spin-echo and Echo-Planar diffusion-weighted MR imaging of tumors of the head and neck. *Acad Radiol* 2019; **26**: e305–16. doi: https://doi.org/10.1016/j.acra.2018.11.016

13. Hiwatashi A, Togao O, Yamashita K, Kikuchi K, Kamei R, Yoshikawa H, et al. Diffusivity of intraorbital lymphoma vs. inflammation: comparison of single shot turbo spin echo and multishot echo planar imaging techniques. *Eur Radiol* 2018; **28**: 325–30. doi: https://doi.org/10.1007/s00330-017-4995-5

14. de Graaf P, Pouwels PJW, Rodjan F, Moll AC, Imhof SM, Knol DL, et al. Single-Shot turbo spin-echo diffusion-weighted imaging for retinoblastoma: initial experience. *AJNR Am J Neuroradiol* 2012; **33**: 110–8. doi: https://doi.org/10.3174/ajnr.A2729

15. Spagnolo F, Caltabiano G, Queirolo P. Uveal melanoma. *Cancer Treat Rev* 2012; **38**: 549–53. doi: https://doi.org/10.1016/j.ctrv.2012.01.002

16. Erb-Eigner K, Willerding G, Taupitz M, Hamm B, Asbach P. Diffusion-weighted imaging of ocular melanoma. *Invest Radiol* 2013; **48**: 702–7. doi: https://doi.org/10.1097/RLI.0b013e31828eea67

17. Heverhagen JT. Noise measurement and estimation in MR imaging experiments. *Radiology* 2007; **245**: 638–9. doi: https://doi.org/10.1148/radiol.2453062151

18. Moon W-J. Measurement of signal-to-noise ratio in MR imaging with sensitivity encoding. *Radiology* 2007; **243**: 908–9. doi: https://doi.org/10.1148/radiol.2433060996

19. Verhappen MH, Pouwels PJW, Ljumanovic R, van der Putten L, Knol DL, De Bree R, et al. Diffusion-weighted MR imaging in head and neck cancer: comparison between half-fourier acquired single-shot turbo spin-echo and epi techniques. *AJNR Am J Neuroradiol* 2012; **33**: 1239–46. doi: https://doi.org/10.3174/ajnr.A2949

20. Kida I, Ueguchi T, Matsuoka Y, Zhou K, Stemmer A, Porter D. Comparison of diffusion-weighted imaging in the human brain using readout-segmented EPI and propeller turbo spin echo with single-shot epi at 7 T MRI. *Invest Radiol* 2016; **51**: 435–9. doi: https://doi.org/10.1097/RLI.0000000000000248

21. Pokorney AL, Miller JH, Hu HH. Comparison of 2D single-shot turbo-spin-echo and spin-echo echo-planar diffusion weighted brain MRI at 3.0 Tesla: preliminary experience in children. *Clin Imaging* 2017; **42**: 152–7. doi: https://doi.org/10.1016/j.clinimag.2016.12.005

22. Schakel T, Hoogduin JM, Terhaard CHJ, Philippens MEP. Technical note: diffusion-weighted MRI with minimal distortion in head-and-neck radiotherapy using a turbo spin echo acquisition method. *Med Phys*

2017; **44**: 4188–93. doi: https://doi.org/10.1002/mp.12363

23. Sigmund EE, Gutman D. Diffusion-weighted imaging of the brain at 7 T with echo-planar and turbo spin echo sequences: preliminary results. *Magn Reson Imaging* 2011; **29**: 752–65. doi: https://doi.org/10.1016/j.mri.2011.02.016

24. Hilbert F, Wech T, Neubauer H, Veldhoen S, Bley TA, Köstler H. Vergleich von turbo spin echo und Echoplanar Bildgebung für Intravoxel incoherent motion und Diffusionstensorbildgebung Der Niere bei 3 tesla. *Z Med Phys* 2017; **27**: 193–201.

25. Helenius J, Soinne L, Perkiö J, Salonen O, Kangasmäki A, Kaste M, et al. Diffusion-Weighted MR imaging in normal human brains in various age groups. *AJNR Am J Neuroradiol* 2002; **23**: 194–9.

26. Foti PV, Farina R, Coronella M, Palmucci S, Montana A, Sigona A, et al. Diffusion-Weighted magnetic resonance imaging for predicting and detecting the response of ocular melanoma to proton beam therapy: initial results. *Radiol Med* 2015; **120**: 526–35. doi: https://doi.org/10.1007/s11547-014-0488-7

27. Kamrava M, Sepahdari AR, Leu K, Wang P-C, Roberts K, Demanes DJ, et al. Quantitative multiparametric MRI in uveal melanoma: increased tumor permeability may predict monosomy 3. *Neuroradiology* 2015; **57**: 833–40. doi: https://doi.org/10.1007/s00234-015-1546-0

28. Foti PV, Longo A, Reibaldi M, Russo A, Privitera G, Spatola C, et al. Uveal melanoma: quantitative evaluation of diffusion-weighted MR imaging in the response assessment after proton-beam therapy, long-term follow-up. *Radiol Med* 2017; **122**: 131–9. doi: https://doi.org/10.1007/s11547-016-0697-3

29. Atlas SW, Braffman BH, LoBrutto R, Elder DE, Herlyn D. Human malignant melanomas with varying degrees of melanin content in nude mice: MR imaging, histopathology, and electron paramagnetic resonance. *J Comput Assist Tomogr* 1990; **14**: 547–54. doi: https://doi.org/10.1097/00004728-199007000-00009

30. DeJordy JO, Bendel P, Horowitz A, Salomon Y, Degani H. Correlation of MR imaging and histologic findings in mouse melanoma. *J Magn Reson Imaging* 1992; **2**: 695–700. doi: https://doi.org/10.1002/jmri.1880020614

31. Ferris JD, Bloom PA, Goddard PR, Collins C. Quantification of melanin and iron content in uveal malignant melanomas and correlation with magnetic resonance image. *Br J Ophthalmol* 1993; **77**: 297–301. doi: https://doi.org/10.1136/bjo.77.5.297

32. Isiklar I, Leeds NE, Fuller GN, Kumar AJ. Intracranial metastatic melanoma: correlation between MR imaging characteristics and melanin content. *AJR Am J Roentgenol* 1995; **165**: 1503–12. doi: https://doi.org/10.2214/ajr.165.6.7484597

33. Premkumar A, Marincola F, Taubenberger J, Chow C, Venzon D, Schwartzentruber D. Metastatic melanoma: correlation of MRI characteristics and histopathology. *J Magn Reson Imaging* 1996; **6**: 190–4. doi: https://doi.org/10.1002/jmri.1880060134

34. Godechal Q, Mignion L, Karroum O, Magat J, Danhier P, Morandini R, et al. Influence of paramagnetic melanin on the MRI contrast in melanoma: a combined high-field (11.7 T) MRI and EPR study. *Contrast Media Mol Imaging* 2014; **9**: 154–60. doi: https://doi.org/10.1002/cmmi.1554

35. Accuracy of diagnosis of choroidal melanomas in the Collaborative ocular melanoma study. COMS report No. 1. *Arch Ophthalmol* 1990; **108**: 1268–73. doi: https://doi.org/10.1001/archopht.1990.01070110084030